SAND99-2466C

ADAPTIVE SPINDLE BALANCING USING MAGNETICALLY LEVITATED BEARINGS*

Patrick Barney[1] , James Lauffer[1], James Redmond[2], William Sullivan[3]

Sandia National Laboratories
Albuquerque, NM 87185
[1]Experimental Structural Dynamics Department MS 0557
[2]Structural Dynamics and Vibration Control Department MS 0847
[3]Mechanical Engineering Department MS 0958

Rebecca Petteys

Department of Mechanical Engineering
Michigan Technological University
Houghton, MI

ABSTRACT

A technological break through for supporting rotating shafts is the active magnetic bearing (AMB). Active magnetic bearings offer some important advantages over conventional ball, roller or journal bearings such as reduced frictional drag, no physical contact in the bearing, no need for lubricants, compatibility with high vacuum and ultra-clean environments, and ability to control shaft position within the bearing. The disadvantages of the AMB system are the increased cost and complexity, reduced bearing stiffness and the need for a controller. Still, there are certain applications, such as high speed machining, biomedical devices, and gyroscopes, where the additional cost of an AMB system can be justified. The inherent actuator capabilities of the AMB offer the potential for active balancing of spindles and micro-shaping capabilities for machine tools. The work presented in this paper concentrates on an AMB test program that utilizes the actuator capability to dynamically balance a spindle. In this study, an unbalanced AMB spindle system was enhanced with an LMS (Least Mean Squares) algorithm combined with an existing PID (proportional, integral, differential) control. This enhanced controller significantly improved the concentricity of an intentionally unbalanced shaft. The study included dynamic system analysis, test validation, control design and simulation, as well as experimental implementation using a digital LMS controller.

INTRODUCTION

There are several advantages of high speed machining such as reduced cutting forces, lower heating rates, and minimal coolant consumption as compared to conventional machining processes. An enabling technology for implementing very high-speed machining is the AMB, which by its high bandwidth error correction capability can minimize dimensional errors while producing superior surface finishes. AMB systems also offer very high speed capabilities without encountering the wear and lubrication problems seen by conventional bearings. Another application for AMB consists of a left-ventricular assist device commonly known as an artificial heart. Here, magnetic bearings offer reliability, very low friction, and their non-contacting nature avoids the generation of life-threatening particles.

A rotary active magnetic bearing typically consists of three or more electromagnets, each of which exerts an attractive force on the ferromagnetic rotor, levitating it without contact. These bearing systems are inherently unstable and control systems are needed to levitate and control the shaft within the magnetic journal. The controller uses position sensors to control the

* Sandia National Laboratories is a multiprogram laboratory operated by Sandia Corporation, a Lockheed Martin Company, for the United States Department of Energy under Contract DE-AC04-94AL85000.

DISCLAIMER

DISCLAIMER

Portions of this document may be illegible in electronic image products. Images are produced from the best available original document.

applied force (coil current) to achieve a desired response. This study involves the design and testing of an LMS digital control algorithm to maintain concentricity of an intentionally unbalanced spindle.

The bearing system used for this study was the MBC500 from Magnetic Moments, Inc. The MBC500 consists of two active magnetic bearings supporting a spindle mounted on top of an anodized aluminum case. The spindle is actively positioned in the radial direction at the bearings and freely rotates about its longitudinal axis. The front panel is a block diagram of the system. BNC connections on the front allow easy access to system inputs and outputs. Each of the four on-board PID controllers can be disabled by switches on the front panel so that an external controller can be implemented. An air turbine drives the shaft to speeds above 40,000 RPM.

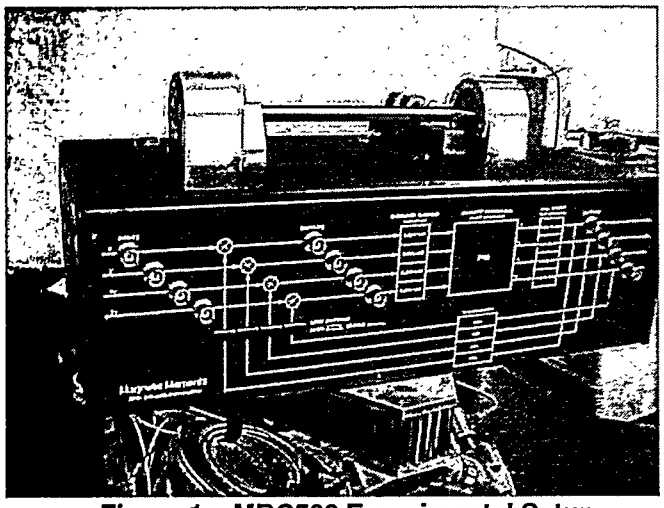

Figure 1 – MBC500 Experimental Setup

A system model was constructed using the analysis and test verification approach. Although the system never goes through a critical speed during this program, it is important to model the spindle flexible body dynamics to obtain good control simulation fidelity. Given the physical properties of the spindle, the free-free modes of the system were modeled and a state space model was produced. This model was validated using experimental modal analysis. The PID control loop was included in the system model. The sensor (eddy-current) and actuator (supporting electromagnets) parameters were modeled, validated and included in the overall system model. Given a steady state rotational speed and a known mass offset, simulations were performed with a rotating force vector at a location of imbalance. Using the simulation system, the PID parameters and adaptive feedforward parameters were optimized for system performance.

The purpose of the simulation was to evaluate alternative control approaches to the imbalance problem of an AMB shaft. Particularly, the LMS algorithm was being evaluated for its performance in a steady state mode of operation. The LMS controller was implemented on the MBC 500 via a PC embedded programmable digital signal processing (DSP) card. Testing of the controlled system at 12,000 rpm indicated that the enhanced controller provided excellent shaft concentricity and performed similar to the simulation.

NOMENCLATURE

x_0	displacement of center of mass of rotor
x_1 and x_2	displacement of rotor at left and right bearings
X_1 and X_2	displacement of rotor at Hall Effect sensors
θ	angle of rotation of rotor about longitudinal axis
F_1 and F_2	forces exerted on rotor at left and right bearings
a_1 and a_2	uncoupled amplitude variables for bending motion
L	total length of rotor
l_1	distance from each bearing to end of rotor
l_2	distance from each sensor to end of rotor
I_0	moment of inertia of rotor around y-axis
m	mass of rotor
M	mass matrix
C	damping matrix
K	stiffness matrix

SYSTEM MODEL

The AMB system was modeled using a general purpose simulation environment (Simulink®). The use of a non-linear simulation environment instead of a linear analysis is due to the nonlinearities in the electromagnets and sensors. The block diagram model of the MBC500 is shown in Figure 2.

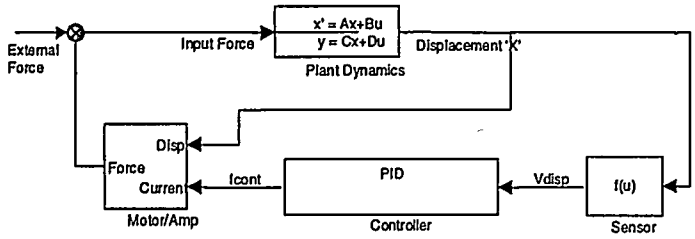

Figure 2 – System block diagram

The shaft was modeled as a simple free-free beam with no gyroscopic effects, i.e. no coupling of the axes due to the rotation of the shaft. The suspected uncoupling of the axes was validated experimentally by comparison of rotating and nonrotating frequency response functions (FRFs). The measured FRFs were compared at the system's first two flexible body resonances and no significant gyroscopic effects were seen.

Plant Dynamics

Both the rigid body and bending modes were incorporated into the simulation. Because the axes are uncoupled, we may look at each independently and can assume that the dynamics in each direction are the same (with the exception of the constant force of gravity in the y-direction). The equations of motion for the rigid body motion, found by balancing the forces and moments about the center of the shaft, are

$$\sum F = m\ddot{x}_0 = F_1 + F_2$$
$$\sum M = I_0\ddot{\theta} = F_2\left(\frac{L}{2} - l_1\right)\cos\theta - F_1\left(\frac{L}{2} - l_1\right)\cos\theta \quad (1)$$

The corresponding state-space system is

$$\begin{bmatrix} \dot{x}_0 \\ \ddot{x}_0 \\ \dot{\theta} \\ \ddot{\theta} \end{bmatrix} = \begin{bmatrix} 0 & 1 & 0 & 0 \\ 0 & 0 & 0 & 0 \\ 0 & 0 & 0 & 1 \\ 0 & 0 & 0 & 0 \end{bmatrix} \begin{bmatrix} x_0 \\ \dot{x}_0 \\ \theta \\ \dot{\theta} \end{bmatrix} + \begin{bmatrix} 0 & 0 \\ 1/m & 1/m \\ 0 & 0 \\ -(L/2-l_1)/I_0 & (L/2-l_1)/I_0 \end{bmatrix} \begin{bmatrix} F_1 \\ F_2 \end{bmatrix} \quad (2)$$

$$\begin{bmatrix} X_1 \\ x_1 \\ X_2 \\ x_2 \end{bmatrix} = \begin{bmatrix} 1 & 0 & -(L/2-l_2) & 0 \\ 1 & 0 & -(L/2-l_1) & 0 \\ 1 & 0 & (L/2-l_2) & 0 \\ 1 & 0 & (L/2-l_1) & 0 \end{bmatrix} \begin{bmatrix} x_0 \\ \dot{x}_0 \\ \theta \\ \dot{\theta} \end{bmatrix}$$

The typical state space representation for this rigid body dynamic equation is

$$\dot{X}_{RB} = A_{RB}X_{RB} + B_{RB}F_{RB}$$
$$Y_{RB} = C_{RB}X_{RB} \quad (3)$$

where 'RB' signifies the rigid body matrices and states.

For rigid body motion, the only restoring forces are those exerted by the magnets, which cannot be included in the linear rigid body state-space model. These AMB forces are used as the inputs (F, usually seen as U) to the state-space model. The state-space outputs (Y) of the system are the positions of the shaft.

The first bending modes were included in this simulation. Since this is an axis-symmetric shaft, each of the flexible body modes are repeated for the X and Y axis; so that including the first two modes actually results in four system modes. Using the shafts mass and inertia properties and an experimentally derived damping, the equation of motion was determined and is shown in matrix form as

$$M\ddot{X} + C\dot{X} + KX = F \quad (4)$$

The state-space system for the flexible body dynamics can be developed in the same manner as the rigid body equations. They are expressed here as

$$\dot{X}_{FB} = A_{FB}X_{FB} + B_{FB}F_{FB}$$
$$Y_{FB} = C_{FB}X_{FB} \quad (5)$$

The inputs (AMB forces, F) and outputs (sensor displacements, Y) for this state-space system must be the same as the rigid body system, but the state vectors are different.

The total displacement of the shaft was found by adding the outputs from each system. In other words,

$$Y_{total} = Y_{RB} + Y_{FB} \quad (6)$$

Sensor Dynamics

The control feedback sensors for this AMB system consist of two orthogonal eddy current proximity probes at each shaft end near the AMB center of force (nearly collocated). The target for the eddy current sensors is the circular shaft that inherently makes the output of voltage versus displacement somewhat non-linear in the operating region. The output voltage is given as

$$V_{sense_i} = 5000X_i + 24\times10^9 X_i^3 \quad (7)$$

Figure 3 provides the displacement versus voltage for a given axis. As can be seen by the plot, the output is relatively linear for small deflections but the nonlinearity becomes more pronounced at the higher displacement levels (hardening spring effect). The range of motion for the MBC500 shaft is .0004 meters; fig. 3 is shown with a range to .0003 meters to de-

emphasize the stronger non-linear affects with displacements above .0003 meters.

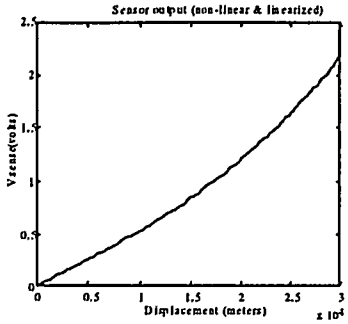

Figure 3 – Eddy current sensor voltage output vs. displacement

Controller Dynamics

There are four independent PID analog controllers supplied with the MBC500. Each controller uses a single axis sensor voltage as input and produces an output voltage. That control output voltage is converted to current and controls the magnet's force for that particular axis. The transfer function for the controller is

$$V_{control} = \left(\frac{1.41(1+8.9\times10^{-4}s)}{(1+3.3\times10^{-4}s)(1+2.2\times10^{-5}s)} \right) V_{sense} \quad (8)$$

The implementation is primarily proportional feedback of the sensor displacement. For a truly co-located sensor-actuator pair and a linear uncoupled system, this is a very robust controller, and for this application it works very well. In essence, the proportional displacement feedback offers a virtual stiffness to the system that results in a bounce mode at about 70 hertz and a pitch mode at about 45 hertz. The non-linearity in the system (mostly due to the actuator) adds effective damping to the system and the result is a well behaved mechanical system.

Active Magnetic Motor Dynamics

The magnets can only exert an attractive force so each bearing consists of four electromagnets - two per set in opposition. A simple cartoon diagram of a single electromagnet is shown in Figure 4.

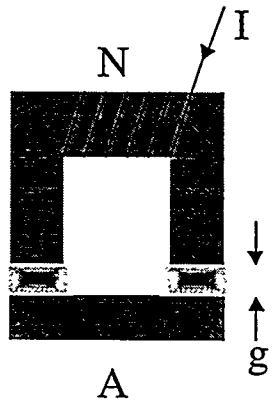

Figure 4 – Simple electromagnet, ferous target and resultant forces.

The force exerted by one electromagnet on the shaft is

$$F = \frac{A\mu_0 N^2 I^2}{4g^2} \quad (9)$$

where A is the cross-sectional area of the magnet, μ_0 is the permittivity of free space, g is the gap between the electromagnet and the rotor, and N is the number of coils in the magnet, each carrying current I.

At equilibrium, the gap is 0.0004 meters and there is a bias current of 0.5 amperes, which is in opposite directions for opposing magnets. If we define k as $A\mu_0N^2/4$ then the total force on the shaft at one bearing due to both magnets (in one axis) is

$$F = k\frac{(I-0.5)^2}{(x+0.0004)^2} - k\frac{(I+0.5)^2}{(x-0.0004)^2} \quad (10)$$

As can be seen by the equation above, the output force of the AMB is highly non-linear with respect to the inputs; the force is proportional to the square of the controller current, and is inversely proportional to the square of the gap. Figure 5 provides an output force map from the actuator as a function of control voltage and shaft displacement. As can be seen by this figure, the output forces become highly non-linear as both the displacement and control voltage become large.

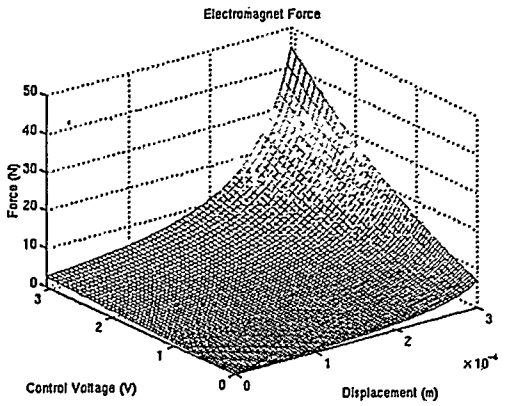

Figure 5 – AMB force output as a function of bearing gap and control voltage.

Modeling the closed loop system

As discussed earlier, a full simulation of the AMB system is necessary because of the nonlinearities in the system. Strong system nonlinearities do not allow for accurate linear analysis when trying to predict the response of a system especially when it is to be used for closed loop control algorithm development. Because of this, a time marching simulation method must be employed to offer reasonable prediction accuracy. Additionally, the operating amplitudes of the simulation must be close to those expected in service (or in the validation experiments) or the resulting predictions may have significant errors. The basic model was first exercised using Simulink® to produce model validation data as presented in the following sections. Next, the model was used to determine the effectiveness of an LMS algorithm for mitigating shaft eccentricity.

System Validation

The validation of a system model for predictive simulation typically requires great effort to achieve. The first step in the process is to determine how success will be qualified in terms of the goal of the prediction and the significance of the error sources. In this case, the purpose of the simulation was to evaluate alternative control approaches to the imbalance problem of an AMB shaft. Particularly, the LMS algorithm was being evaluated for its performance in a steady state mode of operation.

To perform this task, it was assumed that a good representation of the rigid body modes of the system was important. The representation selected for this comparison task was the system FRF from AMB actuator forces to the sensor deflections near a nominal operating amplitude. Figure 6 provides the simulated and measured FRFs for input at one actuator and its respective response. As can be seen by the figure, the model compares well at the resonance. The deviation of the FRF off resonance (especially at the low frequencies) will not particularly affect the response of the LMS imbalance at the selected 200 hertz (12,000 RPM) operating point.

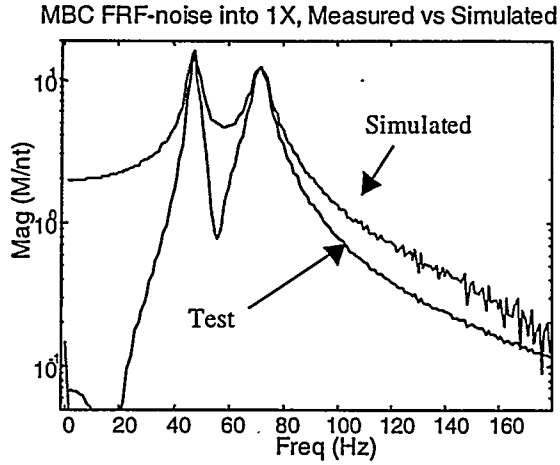

Figure 6 – Measured rigid body FRF versus simulated.

In addition to the rigid body and control dynamics, the flexible body dynamics of the shaft are usually of importance. Although this simulation operates at frequencies well below the lowest flexible body modes, the lowest two were included in the model for completeness. These flexible body dynamics were validated with test. Figure 7 provides the measured and simulated driving point FRFs for one axis. As can be seen by the figure, these functions agree quite well in the regions near the system flexible body modes.

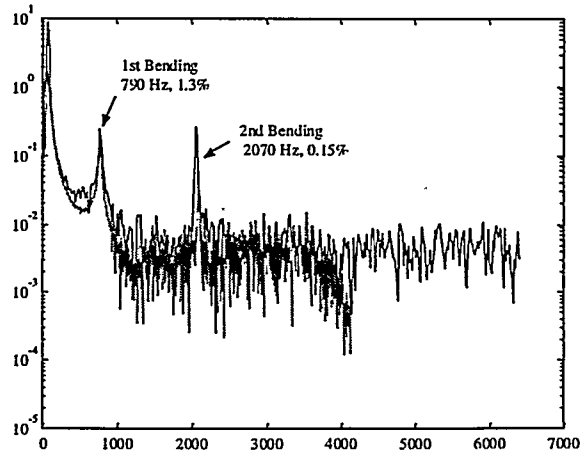

Figure 7 –Simulated versus measured FRF for flexible body modes.

LMS Adaptive Control

The LMS adaptive control strategy is a technique that has received considerable attention over the last 20 years; however, it was the advent of the digital signal processor (DSP) and lower cost system components that has inspired its popularity today. In its primitive state, the LMS algorithm is a gradient descent algorithm used for system identification whose result is used in an FIR implementation to produce a cancellation signal. The cancellation signal is then added to the primary signal (usually mechanically) to produce the resultant error signal which is ideally much smaller than the original primary signal. The modern uses of LMS for active noise cancellation have shown excellent performance for applications such as interior cabin noise cancellation for propeller driven aircraft.

The basic idea of LMS control is shown in Figure 8. As can be seen by this simple diagram, there is a reference signal that is convoluted with a time varying weighting function which produces the output signal (y) which is added to the primary signal (p) to produce the error signal (e).

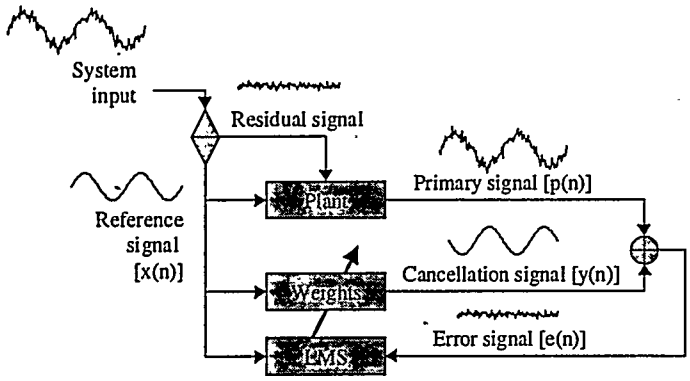

Figure 8 – Functional diagram of the LMS algorithm

The equation below describes the FIR convolution of the current filter weights (w) by the reference signal (x),

$$y(n) = \sum_{i=0}^{N-1} w_i(n) \cdot x(n-i) \qquad (11)$$

where N is referred to as the number of taps.

The kernel of the gradient descent algorithm used to update the weights in the LMS implementation is described in the following equation. As shown, the weights (w) are updated by the current error value (e), the reference vector (x) and a user specified scalar (μ),

$$w_i(n+1) = w_i(n) - \mu \cdot e(n) \cdot x(n-i), i = 0...N-1 \quad (12)$$

The cancellation signal is added to the primary noise signal to produce a resultant error signal which ideally is significantly smaller that the original primary signal. The LMS algorithm is a feed-forward controller (usually inherently stable) but the rapid updating of the weighting function could result in an unstable control. The user's choice of μ, error scaling factors, number of taps (length of the weighting filter) and sample rate all play a significant role in the stability of the implementation.

Application of LMS to AMB

Although the LMS was once seen as a cure all, its commercial implementations have been limited to a few active noise cancellation products. The reason for the lack of customer acceptance appears to be threefold: 1) cost of implementation compared to the alternative passive methods, 2) poor performance due to inappropriate applications and 3) potential for instability. Of the three reasons listed, the inappropriate use of the LMS has been the most significant contributor. Like many new technologies developed for particular applications there is a desire to apply the technique to a much wider field. The practical implementation of the LMS algorithm is particularly well suited for low frequency (below 300 hertz) periodic signals. Ideally, the signal to be controlled would be constructed of one or two primary frequencies with some possible broadband noise. Any potential LMS application should be tested for this at the preliminary stages, followed by examination of the practical aspects.

In the case of the AMB and shaft imbalance, the LMS implementation is a very good fit. Given the nominal operating speed of 12,000 RPM (200 hertz) and a simple imbalance (stationary single sinusoidal) the system meets the primary requirement of low frequency and a few tones. The fact that sensors and actuators already exist for any AMB system makes the implementation very practical. The shaft imbalance problem has an additional advantage in the fact that the system axes are uncoupled so that simple single-input/single-output (SISO) algorithms can be employed reducing the performance requirements for the DSP.

In essence, the out-of-roundness of the shaft is picked up by the displacement sensor in the AMB bearing, this signal becomes the error signal (primary signal) to be minimized. Given that the signal can be minimized, then the shaft would become more geometrically centered with respect to the bearing housing.

LMS Simulation

The basic time domain LMS algorithm was implemented in both simulation and experiment. The LMS system model utilized the validated Simulink® model as a basis with the addition of a imbalance forcing function and an LMS

feedforward algorithm. The figure below provides the block diagram for the LMS system model.

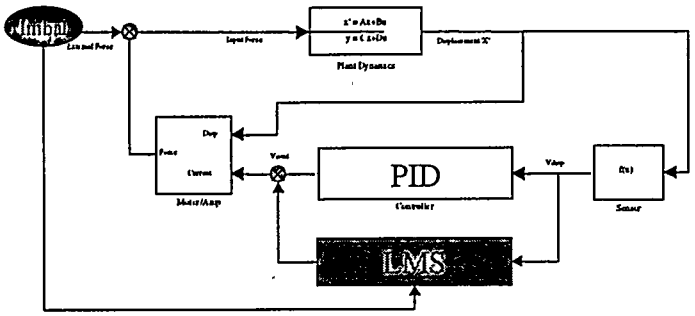

Figure 9 – Block diagram of AMB controller with LMS algorithm and imbalance excitation force.

As can be seen by the figure, there is the basic PID inner loop with the additional LMS control loop wrapped around it. In the case of the simulation, the standard SISO digital implementation of the LMS was implemented. In this particular case, the bearing 1 X axis was chosen, although the simulation predicted the responses in all axes.

The required inputs to the LMS algorithm are the reference signal and the error signal. In this simulation, a sinusoidal forcing function was generated at a frequency (200 hertz) and amplitude consistent with the test configuration. The forcing function generated simulated a mass imbalance at the bearing 1 X and Y axes. This forcing function was also used as the LMS reference signal because it was be coherent with the error signal to be attenuated. In practice, the equivalent quality signal is derived from the tachometer. The error signal was the simulated voltage from the eddy current sensor located at 1 X. The resultant LMS output signal was added to the control voltage into the AMB.

The LMS parameters investigated during the control algorithm development included the effective sample rate of the analog-to-digital (A/D) converter, the number of taps of the weighting vector and the convergence coefficient (μ).

Figure 10 provides a summary of the results of the simulation. Again, the imbalance was simulated at one end of the shaft in both directions. The upper plot is the X displacement versus time, while the lower plot is the Y displacement versus time. At the start of the simulation, both axes have equal sinusoidal runnout (.000075 meters) due to the imbalance. As seen by the X displacement (the control axis), the LMS control quickly moves towards reduction of the error signal. At the end of the three second simulation, the error signal is attenuated by a factor of ten. The cross axis coupling (to the Y axis) is near zero as seen by the fact that the uncontrolled Y axis is not affected by the control forces injected at the X axis.

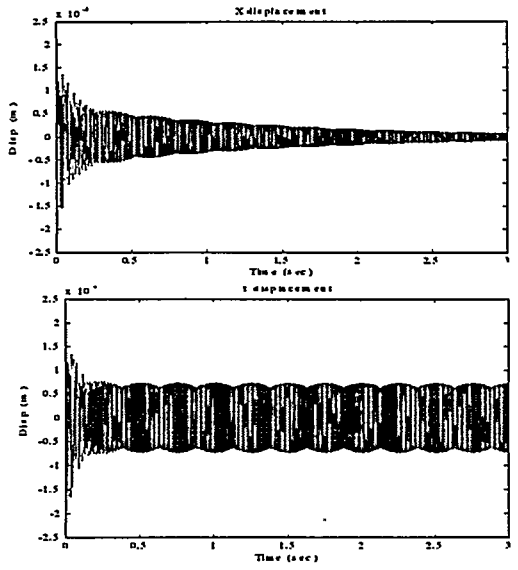

Figure 10 – Simulated system response for LMS control convergence.

LMS Experiment

The basic time domain LMS algorithm was implemented in experiment using the MBC500 and the LMS concept used for the simulation. The natural imbalance of the shaft was sufficient for reasonable eccentric rotation at 12,000 RPM. The test used a single operating speed of 12,000 RPM, a tachometer signal as the reference signal and a small shaft imbalance as the forcing function. The once per revolution tachometer provided a very clean signal which was coherent with the imbalance as required for LMS.

The PC-based DSP system was programmed for a SISO LMS with the capability to update μ in real-time. The nominal parameters arrived at in simulation were used as the baseline DSP implementation and are given in Table 1

Table 1 – DSP parameters determined from simulation.

sample frequency	2000 Hz
Filter length (w)	20 taps
μ	Variable
Reference	Tachometer

As shown in the table, μ was selected as variable to account for scaling issues within the A/D of the DSP.

Figure 11 provides a summary of the results of the test. The upper plot is the X displacement (volts) versus time, while the lower plot is the Y displacement (volts) versus time. At the start of the simulation, both axes have equal sinusoidal run-out (.000075 meters) due to the imbalance. As seen by the X

displacement (the control axis), the LMS control quickly attenuates the error signal (orders of magnitude). The cross axis coupling (to the Y axis) is near zero as seen by the fact that the uncontrolled Y axis is not affected by the control forces injected at the X axis.

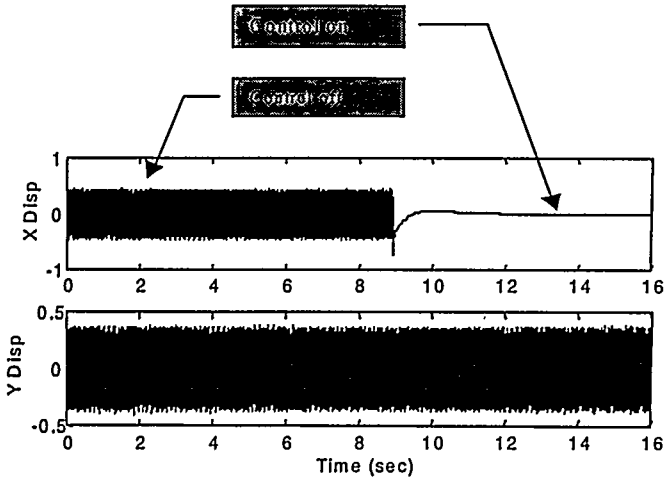

Figure 11 – Experimental result summary for LMS implementation on AMB shaft imbalance (control on versus control off).

Compared to the simulation, the results of this test are very good and converge even more quickly. The reason for the quicker convergence is that the μ used in the test was higher than that of the simulation. Although the attenuation of the imbalance is fast, the impulsive nature of the control force when first activated causes a rigid body motion which takes a few seconds to settle out.

Conclusions

The work presented in this paper concentrated on an AMB test program that utilized the actuator capability to dynamically balance a spindle. An unbalanced AMB spindle system was enhanced with an LMS (Least Mean Squares) algorithm wrapped over an existing PID rigid body controller. The enhanced controller improved the concentricity of the MBC500 imbalanced shaft by two orders of magnitude. It should be noted here that although the shaft becomes less eccentric with this control, the imbalance forces on the shaft ($Mr\omega^2$) may not be significantly reduced.

The methods and the implementation of predictive simulation, model validation and test implementation were shown here to be useful for control algorithm development. Additional efforts will be pursued which address: multiaxis control, high slew rate operations, and alternative error signals. The LMS control approach of AMB systems presented in this paper are extendable to reduction of forces into the bearing housing (a notch filter) and possibly force minimization through critical speed resonance.

ACKNOWLEDGMENTS

The authors wish to thank Professor Brad Paden of the University of California at Santa Barbara and Magnetic Moments, Inc. and Professor Gordon Parker at Michigan Technological University for their contributions to this project.

REFERENCES

Paden, B., "Operating Manual for the MBC500", Magnetic Moments Inc., Santa Barbara CA.

Lueg, P., June 1936 "Process of Silencing Sound Oscillations," U.S. Patent No. 2,043,416.

Widrow, B., and S. D. Stearns, 1985, "Adaptive Signal Processing", Prentice-Hall, Englewood Cliffs, NJ.

Elliott, S. J., P. A. Nelson, I. M. Stothers and C. C. Boucher, 1990, "In-Flight Experiments on the Active Control of Propeller-Induced Cabin Noise", Journal of Sound and Vibration, Vol. 140, No. 2. pp. 219–238.

Kuo, S. M., and C. Chen, 1990, "Implementation of Adaptive Filters with the TMS320C25 or the TMS320C30," Digital Signal Processing Applications with the TMS320 Family, Volume 3, edited by P. Papamichalis, Prentice-Hall, Englewood Cliffs, NJ, pp. 191–271.